ISSN 0081-5438, Proceedings of the Steklov Institute of Mathematics, 2023, Vol. 322, pp. 4–17. © Pleiades Publishing, Ltd., 2023.
Russian Text © The Author(s), 2023, published in Trudy Matematicheskogo Instituta imeni V.A. Steklova, 2023, Vol. 322, pp. 10–23.

Linear and Nonlinear Development of Bending Perturbations in a Fluid-Conveying Pipe with Variable Elastic Properties

K. E. Abdul'manov[a] **and V. V. Vedeneev**[b]

Received January 29, 2023; revised February 28, 2023; accepted May 20, 2023

Abstract—We consider bending vibrations of a fluid-conveying pipe resting on an elastic foundation with nonuniform elasticity coefficient. Previously A. G. Kulikovskii showed analytically that the elasticity parameters can be distributed in such a way that at every point the system is either locally stable or convectively unstable. In this case, despite the absence of local absolute instability, there exists a global growing mode whose formation is associated with the points of internal reflection of waves. In the present paper, we perform a numerical simulation of the development of the initial perturbation in such a system. In the linear formulation we demonstrate how the perturbation is transformed into a growing eigenmode after a series of reflections and passages through a region of local instability. In the nonlinear formulation, where the nonlinear tension of the pipe is taken into account within the von Kármán model, we show that the perturbation growth is limited; in this case the vibrations acquire a quasi-chaotic character but do not leave the region bounded by the internal reflection points determined by the linearized problem.

DOI: 10.1134/S0081543823040028

1. INTRODUCTION

In [6], Kulikovskii studied the natural bending vibrations of a nonuniform elastic pipe filled with a flowing fluid by the analytic WKB method (Fig. 1). The pipe was characterized by a bending stiffness D that was a function of the spatial coordinate and varied slowly according to a quadratic law. The dispersion equation is of the fourth order in the wave number k, so there exist four spatial waves $k_i(\omega)$, $i = 1, \dots, 4$. It was demonstrated that for a certain choice of the parameters, there exists a region $-A_2 < x < A_2$ in which the pipe is locally unstable and there are internal reflection points (turning points in terms of the WKB method) $x = \pm A_3$, $|A_3| > |A_2|$. In this case there arises a system of three waves transforming into each other that form an eigenfunction with the following structure:

- the wave corresponding to the wave number k_2 propagates from left to right; moreover, for $x < -A_2$, the wave number k_2 is real;
- upon passing through the point $x = -A_2$, this wave turns into one growing and one decaying wave (complex conjugate k_1 and k_2); the k_1 wave grows in the interval $-A_2 < x < A_2$, which contains the origin;
- upon passing through the point $x = A_2$, these waves turn into two waves with real k_1 and k_2, with the amplitude of the k_2 wave being greater than its amplitude before the amplification interval $-A_2 < x < A_2$;

[a] Faculty of Mechanics and Mathematics, Lomonosov Moscow State University, Moscow, 119991 Russia.
[b] Steklov Mathematical Institute of Russian Academy of Sciences, ul. Gubkina 8, Moscow, 119991 Russia.
E-mail addresses: abdulmanov.kirill@gmail.com (K. E. Abdul'manov), vasily@vedeneev.ru (V. V. Vedeneev).

Fig. 1. Pipe with a flowing fluid on an elastic foundation.

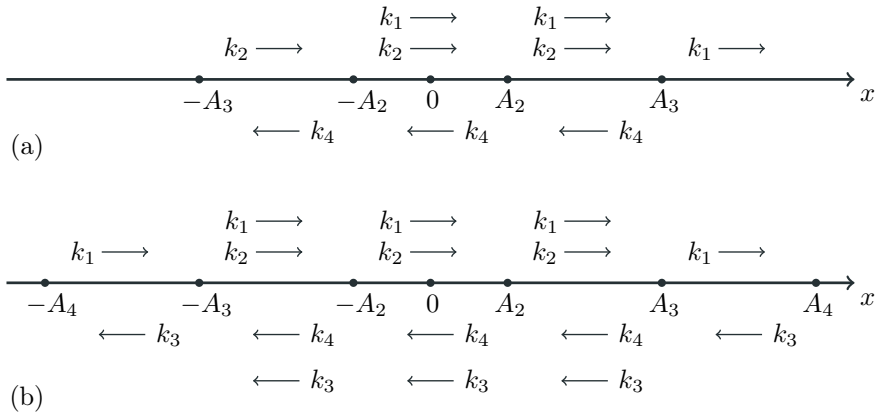

Fig. 2. The structure of wave propagation and turning points: (a) in the original formulation [6] and (b) after modification.

- the k_2 wave is reflected from the point $x = A_3 > A_2$ and turns into a k_4 wave propagating in the opposite direction (to the left);
- in turn, the k_4 wave is reflected from the symmetric point $x = -A_3$ and turns into the k_2 wave; then the cycle of reflections is repeated;
- the k_1 wave leaves the interval $(-A_3, A_3)$ and propagates indefinitely to the right.

Thus, there is a closed cycle of reflections of waves from the turning points $x = \pm A_3$. The cycle is shown schematically in Fig. 2a. In each cycle, the amplitudes increase when the waves pass through the interval $(-A_2, A_2)$, and the wave corresponding to k_1 is emitted and propagates indefinitely to the right.

The goal of the present study is to numerically simulate the above-mentioned process, in which we also take account of nonlinear terms. Note, however, that the emission of the k_1 wave propagating indefinitely in the direction of $x \to +\infty$ makes it difficult to set the boundary condition in numerical simulation. To overcome this difficulty, we have modified the problem as follows: instead of dealing with the nonuniform bending stiffness of the pipe considered in [6], we assume that the stiffness F of the elastic foundation is nonuniform and varies according to the same quadratic law. In this case there also arises a system of four waves transforming into each other, but now the k_1 wave does not just leave the region $(-A_3, A_3)$ but is reflected from the new turning point $x = A_4 > A_3$ and turns into a wave with real k_3 that propagates to the left. In turn, the latter wave is reflected from the symmetric point $x = -A_4$ and turns into a wave with real k_1 that propagates to the right. Thus, after this modification, the whole vibration of the pipe is localized in the interval $-A_4 < x < A_4$ (Fig. 2b). Imposing any boundary conditions at points away from $(-A_4, A_4)$ makes it possible to numerically observe the cycle of growing waves transforming into each other that form an eigenfunction.

Below, at the first stage, we numerically study the nonlinear problem describing the development of a perturbation in a fluid-conveying pipe that lies on a nonuniform elastic foundation in the case where the local stability or convective instability condition holds at all points. We show that in this case a global eigenfunction is formed, which confirms the analytic constructions of [6].

At the second stage, we introduce nonlinearity arising due to tensile stresses caused by bending (von Kármán model of large deflections) into the original problem. We perform numerical simulation of the development of a perturbation under the same conditions as at the first stage.

This problem attracts interest because the growing global eigenmode constructed in [6] does not require the existence of a local absolute instability region: all points of the pipe exhibit either convective instability or stability. At the same time, as proved in [2, 8], the presence of a local absolute instability is a necessary condition for the existence of a growing global eigenmode for second-order systems, i.e., for systems with two spatial waves. In a number of particular problems, including the axially symmetric flows of a fluid in elastic tubes [16], the onset of the von Kármán vortex street in the cylinder wake [9, 10], and hot jets [3], it has also been proved that the instability of an inhomogeneous system occurs only in the presence of a local absolute instability region. Kulikovskii showed in [6] that in the case of interaction of more than two waves, a growing global eigenmode can exist even without local absolute instability; i.e., the results of [2, 8] are not generally valid for systems of order higher than 2. For second-order systems, possible forms of nonlinear global eigenmodes, i.e., neutral oscillations of a nonlinear inhomogeneous system, were previously studied in [11–13]. In all the found types of modes, the positions of the leading and trailing edges of the perturbation are determined by the conditions dictated by the purely linear problem, while the nonlinearity determines the behavior of the perturbation only in its central part. It is of interest to find out whether this property extends to the nonlinear problem considered in the present paper, in which not only there are more than two spatial waves, but also the nonlinearity exhibits qualitatively different behavior.

2. LINEAR PROBLEM

2.1. Statement of the problem. Consider the problem of transverse vibrations of a pipe resting on an elastic foundation and conveying an ideal incompressible fluid. The x axis is directed along the unperturbed rectilinear axis of the pipe. The transverse displacement $w(x,t)$ of the pipe satisfies the equation [5]

$$\rho_1\frac{\partial^2 w}{\partial t^2}+\rho_2\left(\frac{\partial}{\partial t}+v\frac{\partial}{\partial x}\right)^2 w=-Fw-D\frac{\partial^4 w}{\partial x^4}, \tag{2.1}$$

where ρ_1 and ρ_2 are the masses per unit length of the pipe and the fluid, respectively, v is the fluid velocity, F is the stiffness of the elastic foundation, and D is the bending stiffness of the pipe (all quantities are assumed to be dimensionless).

The pipe is clamped on both sides; i.e., the boundary conditions have the form

$$w(x,t)\big|_{x=\pm L/2}=\left.\frac{\partial w(x,t)}{\partial x}\right|_{x=\pm L/2}=0, \tag{2.2}$$

where L is the pipe length. The initial conditions are

$$w(x,0)=w_0(x),\qquad \frac{\partial w(x,0)}{\partial t}=w_1(x). \tag{2.3}$$

When we consider the wave motion $w(x,t)=Ae^{i(kx-\omega t)}$, the dispersion equation corresponding to equation (2.1) and solved for ω has the form

$$\omega=Uk\pm\sqrt{Qk^4-Pk^2+R(x)}, \tag{2.4}$$

where

$$U=\frac{\rho_2 v}{\rho_1+\rho_2},\qquad P=\frac{\rho_1\rho_2 v^2}{(\rho_1+\rho_2)^2},\qquad Q=\frac{D}{\rho_1+\rho_2},\qquad R(x)=\frac{F(x)}{\rho_1+\rho_2}.$$

We assume that the elasticity coefficient of the foundation is distributed nonuniformly according to the law $R(x) = A + Bx^2$, and U, P, Q, A, and B are positive constants, with A and B assumed to be small. From a physical point of view, such a function $R(x)$ means the weakening of the restoring force near the origin.

2.2. Turning points. Let $\omega(k) = Uk \pm \sqrt{Qk^4 - Pk^2 + A + Bx^2}$. Consider the graph of the function $\omega(k)$ for real k and $x = 0$ (Fig. 3). All graphs here and in what follows are plotted for the following parameters of the problem:

$$\rho_1 = 0.1, \quad \rho_2 = 0.9, \quad v = 8, \quad D = 7, \quad A = 0.1, \quad B = 0.002.$$

The value of $A = R(0)$ is chosen so that the inequality $Qk^4 - Pk^2 + R(x) < 0$ holds at $x = 0$ in some interval of values of k (Fig. 3), which vanishes with increasing x. Thus, in a neighborhood of the origin the system exhibits instability. The parameter B is taken to be small to ensure a slow variation of the function $R(x)$. To ensure the growth of the eigenmode constructed in [6] in the form of a chain of waves transforming into each other, it is necessary that the frequency ω should correspond to values from the range $\omega_1 < \omega < \omega_2$ in Fig. 3. In this case the local growth of perturbations occurs near the origin ($\operatorname{Im} k < 0$ for a wave propagating from left to right); moreover, the condition of local convective instability $\rho_1/\rho_2 < 1/8$ holds at all points (see [7]). Next, for calculations we take the value

$$\omega = \omega_0 = 3.266,$$

which is shown in Fig. 3.

In the plane of real k and x (Fig. 4) the curve $\omega(k, x) = \omega_0$ has a shape that ensures the growth of perturbations near the origin.

The turning points, i.e., the values of x that correspond to the branching of the function $k(\omega)$ at a given frequency ω_0, can be found as follows. The coordinate x is a parameter in the dispersion

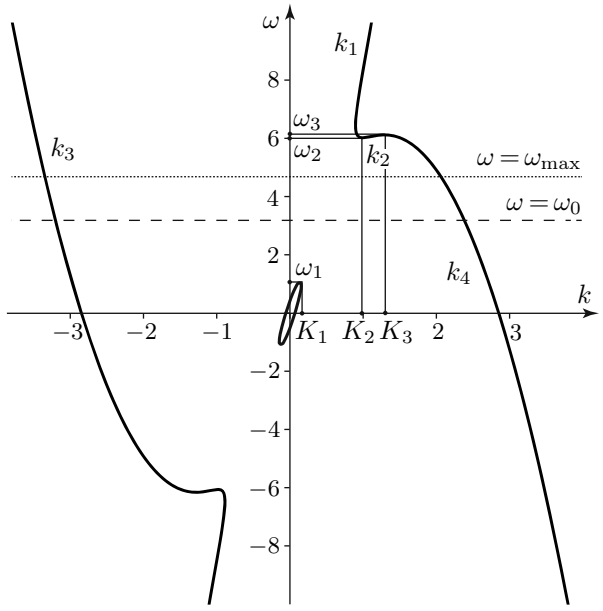

Fig. 3. Dispersion curve $\omega(k)$ for $x = 0$.

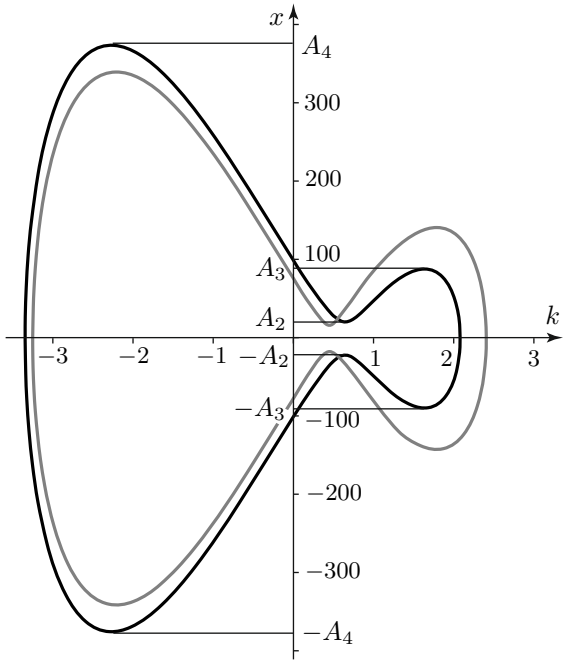

Fig. 4. The function $x(k)$ for $\omega = \omega_0$ (gray curve) and $\omega = \omega_{\max}$ (black curve).

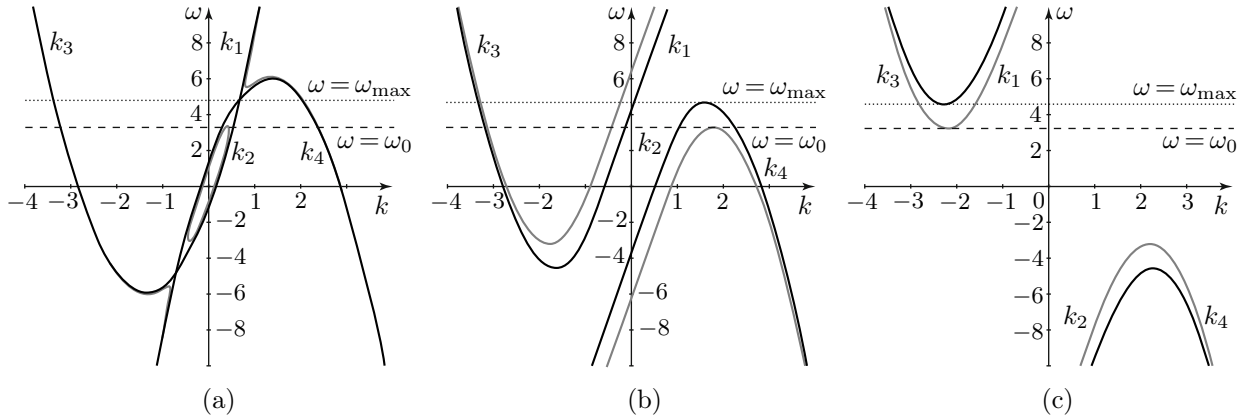

Fig. 5. Dispersion curve for $\omega = \omega_0$ (gray) and $\omega = \omega_{\max}$ (black): (a) for $x = A_2(\omega)$, (b) for $x = A_3(\omega)$, and (c) for $x = A_4(\omega)$.

relation (2.4). Gradually increasing the value of x, we find all the necessary points:

(1) The straight line $\omega = \omega_0$ is tangent to the branches of the graph of $\omega(k)$ at $x = A_2(\omega_0) = 19.5$ (Fig. 5a). In the interval $-A_2 < x < A_2$, the k_1 wave experiences a spatial growth.

(2) One of the branches of $\omega(k)$ is tangent to the straight line $\omega = \omega_0$ at $x = A_3(\omega_0) = 139.8$, which corresponds to the first internal reflection point A_3 (Fig. 5b). The k_2 wave is reflected from the point A_3, turns into the k_4 wave, and propagates in the opposite direction to the point $-A_3$, where it transforms back into the k_2 wave.

(3) The other branch of $\omega(k)$ is tangent to the straight line $\omega = \omega_0$ at $x = A_4(\omega_0) = 338.3$, which corresponds to the second internal reflection point A_4 (Fig. 5c). The k_1 wave is reflected from the point A_4, turns into the k_3 wave, and propagates in the opposite direction to the point $-A_4$, where it transforms into the k_1 wave.

Alternatively, one can find all turning points by fixing $\omega(k, x) = \omega_0$ and solving the equation $\partial\omega/\partial k = 0$ for x. The graph of the function $x(k)$ and the positions of the turning points are shown in Fig. 4.

Notice that the chosen frequency ω_0 is not the most rapidly growing one and does not correspond to the maximum length of the growth interval on the x axis. The longest growth interval is provided by the frequency

$$\omega = \omega_{\max} = 4.618,$$

which corresponds to the merging of the branches in the graph of $\omega(k)$ (Fig. 5a) and the vanishing of the instability region with increasing x. For the frequency $\omega_{\max}$ we have

$$A_2(\omega_{\max}) = 23.3, \qquad A_3(\omega_{\max}) = 90.7, \qquad A_4(\omega_{\max}) = 376.2.$$

2.3. Finite-difference scheme for the equation of vibrations of a fluid-conveying pipe on a nonuniform foundation. Let us construct a finite-difference scheme for equation (2.1), which we rewrite as

$$D\frac{\partial^4 w}{\partial x^4} + (\rho_1 + \rho_2)\frac{\partial^2 w}{\partial t^2} + 2\rho_2 v\frac{\partial^2 w}{\partial x \partial t} + \rho_2 v^2\frac{\partial^2 w}{\partial x^2} + Fw = f(x,t), \tag{2.5}$$

where $F(x) = (A + Bx^2)(\rho_1 + \rho_2)$ and $f(x,t)$ is the body force added to the right-hand side, which will be used below to introduce a perturbation. We define a uniform grid in x and t:

$$x_m = -\frac{L}{2} + mh, \quad m = 0, \dots, M, \quad h = \frac{L}{M}, \qquad t_n = n\tau, \quad n = 0, \dots, N, \quad \tau = \frac{t_N - t_0}{N},$$

where M is even.

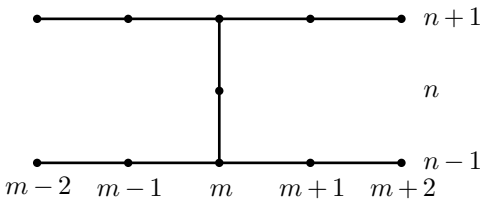

Fig. 6. Stencil of the finite-difference scheme.

Let us approximate the derivatives by finite differences up to orders $O(\tau^2)$, $O(\tau h)$, $O(h^2)$, and $O(h^2)$ according to the stencil shown in Fig. 6. Denoting $w(x_m, t_n)$ by w_m^n, we have

$$\frac{\partial^2 w}{\partial t^2} = \frac{w_m^{n+1} - 2w_m^n + w_m^{n-1}}{\tau^2}, \qquad \frac{\partial^2 w}{\partial t \partial x} = \frac{w_{m+1}^{n+1} + w_{m-1}^{n-1} - w_{m+1}^{n-1} - w_{m-1}^{n+1}}{4\tau h},$$

$$\frac{\partial^2 w}{\partial x^2} = \frac{\left(w_{m-1}^{n+1} - 2w_m^{n+1} + w_{m+1}^{n+1}\right) + \left(w_{m-1}^{n-1} - 2w_m^{n-1} + w_{m+1}^{n-1}\right)}{2h^2},$$

$$\frac{\partial^4 w}{\partial x^4} = \frac{\left(w_{m-2}^{n+1} - 4w_{m-1}^{n+1} + 6w_m^{n+1} - 4w_{m+1}^{n+1} + w_{m+2}^{n+1}\right) + \left(w_{m-2}^{n-1} - 4w_{m-1}^{n-1} + 6w_m^{n-1} - 4w_{m+1}^{n-1} + w_{m+2}^{n-1}\right)}{2h^4}.$$

Substituting these formulas into equation (2.5), we obtain finite-difference equations for the interior grid points with $m = 2, \ldots, M-2$ and $n = 2, \ldots, N$.

As said above, the perturbation is introduced via the body force; therefore, we use the zero initial conditions $w_0(x) = w_1(x) = 0$ in the calculations. Then the initial and boundary conditions for the finite-difference problem have the form

$$w(x,0) = w_m^0 = 0, \qquad \left.\frac{\partial w}{\partial t}\right|_{t=0} = \frac{w_m^1 - w_m^0}{\tau} = 0, \tag{2.6}$$

$$w_0^{n+1} = w_N^{n+1} = 0,$$

$$\left.\frac{\partial w}{\partial x}\right|_{x=-L/2} = \frac{w_1^{n+1} - w_0^{n+1}}{h} = 0, \qquad \left.\frac{\partial w}{\partial x}\right|_{x=L/2} = \frac{w_N^{n+1} - w_{N-1}^{n+1}}{h} = 0. \tag{2.7}$$

Since, as shown below, the perturbations do not interact with the boundaries of the computation domain, the lower order of approximation $O(h)$ of the boundary conditions does not reduce the approximation order of the whole problem.

In each time layer, the equations obtained form a closed system of linear algebraic equations for the unknowns $(w_0^{n+1}, w_1^{n+1}, \ldots, w_M^{n+1})^{\mathrm{T}}$, which is solved by the pentadiagonal matrix algorithm [1].

We introduce the perturbation locally at the center of the pipe by an additional external body force on the right-hand side of equation (2.5) with density

$$f(x_m, t_n) = \begin{cases} \dfrac{0.05}{h} \sin(\omega_0 t_n)\, \Theta(t_n) & \text{for } m = \dfrac{M}{2}, \\ 0 & \text{otherwise}, \end{cases} \tag{2.8}$$

$$\Theta(t_n) = \begin{cases} 1 & \text{for } t_n < t^*, \\ 0 & \text{for } t_n \geq t^*, \end{cases} \qquad t^* = 10\frac{2\pi}{\omega_0};$$

i.e., we define a sinusoidal excitation with frequency ω_0 that acts for ten vibration periods and is turned off after that.

The computer program that solves the problem was tested for convergence with respect to the space and time steps and checked on the problem of simulation of eigenfrequencies and vibration modes of an empty uniform pipe and on the problem of determining the boundary of the abso-

lute/convective instability of a uniform fluid-conveying pipe. In all the cases the results of calculations coincided with the theory.

2.4. Results of calculations. The spatial domain $[-700, 700] \ni x$ in the calculations was chosen with a margin so that one could observe the almost complete damping of vibrations outside the interval $-A_4 < x < A_4$. The perturbation has ten vibration periods and mostly propagates to the right, although there is a perturbed region of small amplitude that moves to the left. Upon leaving the growth region $-A_2 < x < A_2$, the perturbation represents a "wave train" containing both right-propagating waves k_1 and k_2. The calculations show that part of the perturbation (corresponding to k_2) does not propagate beyond the point A_3 and is reflected from it, while the other part (corresponding to k_1) propagates further and is reflected from the point A_4 (Fig. 7). The reflected waves (corresponding to the wave numbers k_4 and k_3) propagate to the left and are reflected from the points $-A_3$ and $-A_4$, as expected from theoretical considerations.

While passing through the interval $(-A_2, A_2)$, the numerically calculated perturbation grows, which is consistent with the theory. Since the perturbation splits into several independent wave trains and they pass through the growth interval at different time points, the growth of perturbations is observed intermittently: there is a time interval of growth, then the growth stops for some time, and later it resumes again. Figure 8 demonstrates the typical state of the perturbed pipe before and after a particular time interval of growth.

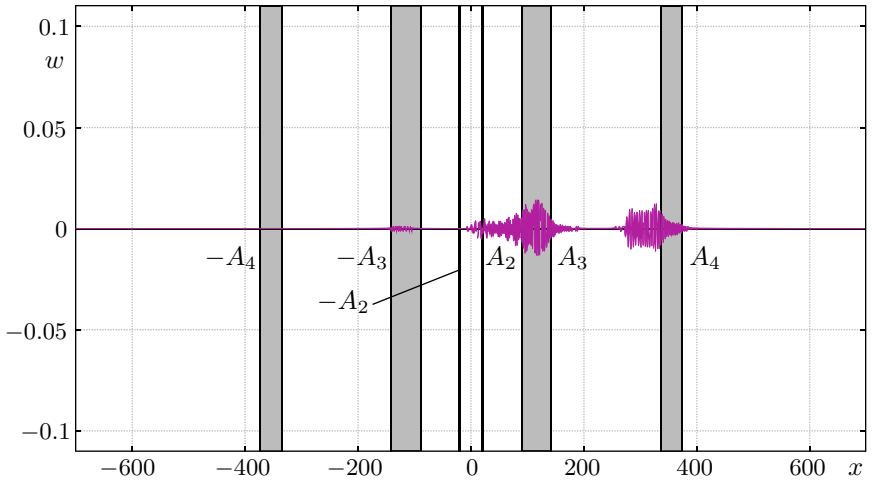

Fig. 7. Reflection from the points A_3 and A_4, $t = 59.5$. The gray strips are the location ranges of the points $\pm A_2(\omega)$, $\pm A_3(\omega)$, and $\pm A_4(\omega)$ for $\omega_0 \le \omega \le \omega_{\max}$.

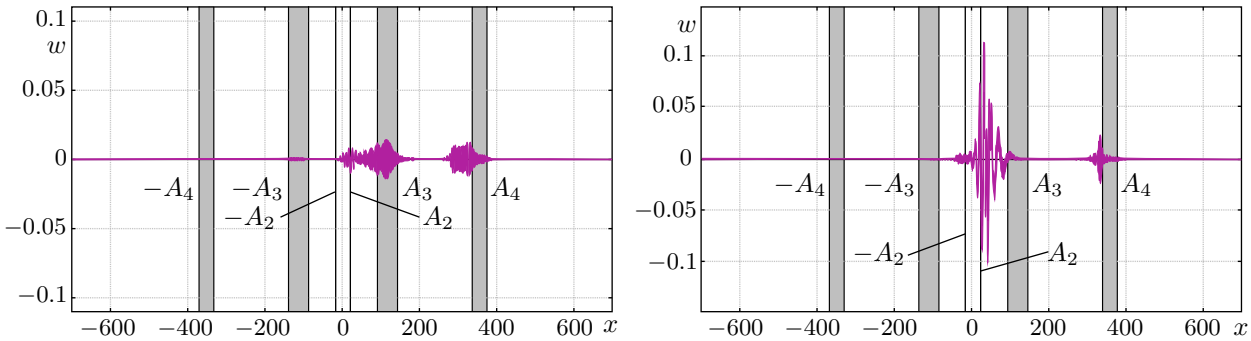

Fig. 8. Perturbation at time points corresponding to (a) the beginning $t = 61$ and (b) the end $t = 73.5$ of an individual growth period of the perturbation.

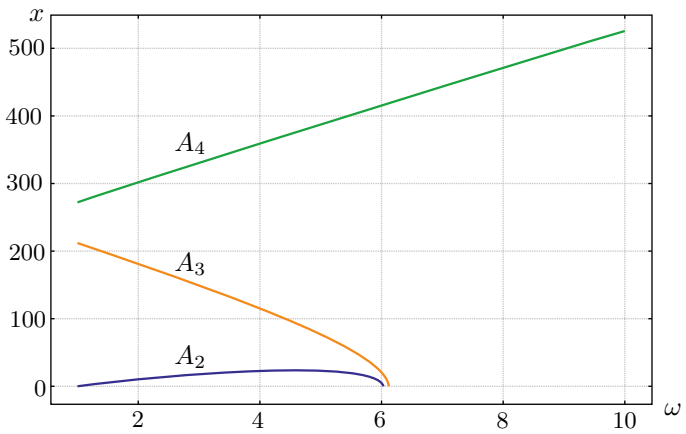

Fig. 9. The functions $A_2(\omega)$, $A_3(\omega)$, and $A_4(\omega)$.

Figures 7 and 8 show that part of the perturbation nevertheless propagates slightly beyond the points $A_3(\omega_0)$ and $A_4(\omega_0)$. This is associated with the fact that the given localized perturbation of frequency ω_0 acts during a finite time interval $0 < t < t^*$. Obviously, the dominant frequency in this interval is ω_0, but there are inevitably other frequencies. The perturbations with higher frequencies $\omega > \omega_0$ are reflected at points A_4 and A_3 that are, respectively, farther from and closer to the center of the pipe. The positions of these points as functions of the frequency ω are depicted in Fig. 9.

Although the components with higher frequencies $\omega \sim \omega_{\max} > \omega_0$ have a small initial amplitude, they eventually become dominant due to their higher growth rate. As a result, the positions of the turning points also slightly shift. For this reason, in Fig. 7 and the subsequent figures we indicate the location intervals of the turning points $A_3(\omega)$ and $A_4(\omega)$, as well as the boundaries of the growth region $A_2(\omega)$, in the frequency range $\omega_0 \le \omega \le \omega_{\max}$.

Nevertheless, the calculations show that the perturbation does not propagate beyond certain boundaries on the x axis even for sufficiently large t. We can expect that this is so due to the boundedness of the initial frequency spectrum of the perturbation.

To confirm this conjecture, we constructed discrete spectra of the perturbation (using the discrete Fourier transform) on the interval $0 < t < T$, where T is the time point of interest, at the points x_1, x_2, x_3, and x_4:

$$A_2 < x_1 = 100 < A_3 < x_2 = 300 < A_4 < x_3 = 380 < x_4 = 415.$$

Figure 10 shows the most interesting range of frequencies from 0 to 12. Figure 10a corresponds in time to Fig. 7, and one can see from it that before the reflection point A_4 (the curve corresponding to $x_2 = 300$) the spectrum contains waves with frequencies $\omega > \omega_0$; hence, these waves will be reflected from $x = A_4(\omega_0) = 338.3$ farther downstream than expected. This can be observed in Fig. 7.

Based on the shape of the spectrum at time $t = 360$ (Fig. 10b), we can conclude that the initial spectrum with dominant frequency ω_0 eventually transforms into spectrum with higher frequencies $\omega \sim \omega_{\max}$, which have a higher growth rate and therefore become dominant. The final form of the perturbation contains waves with frequencies different from ω_0, up to $\omega \approx 5.7$. According to Fig. 9, perturbations with these frequencies must not propagate beyond the point $A_4 \approx 406$. The calculations did not reveal the propagation of perturbations beyond this point either.

Over a long time interval after several cycles of reflections and growth, the initial perturbation gradually takes the shape shown in Fig. 11. After that this perturbation hardly changes its shape but indefinitely increases with time since the problem is linear. Thus, the numerically calculated evolution of the perturbation is consistent with the theoretically expected behavior.

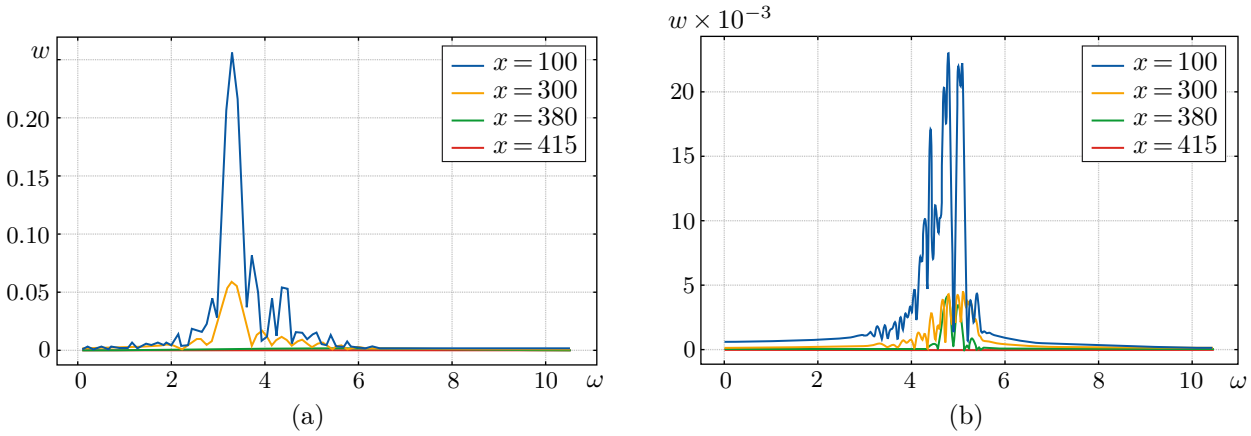

Fig. 10. Discrete spectrum at time points (a) $t = 59.5$ and (b) $t = 360$.

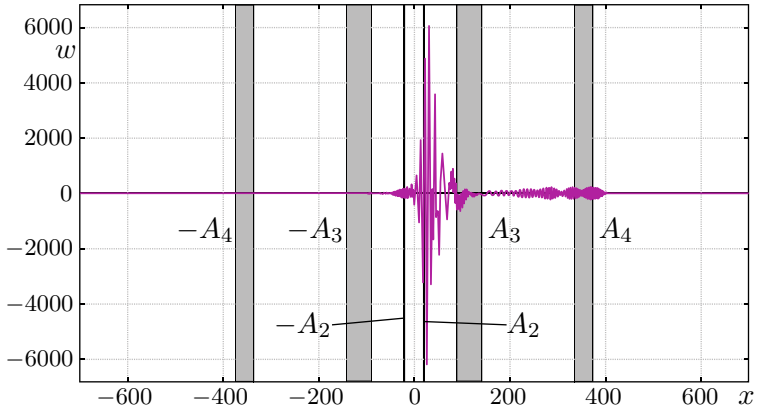

Fig. 11. Perturbation $w(x,t)$ at $t = 318.5$.

3. NONLINEAR PROBLEM

3.1. Statement of the problem. Since in reality a perturbation cannot grow indefinitely, we consider an additional nonlinear tension of the pipe due to its bending according to the von Kármán model of large deflections [17]:

$$\rho_1 \frac{\partial^2 w}{\partial t^2} + \rho_2 \left(\frac{\partial}{\partial t} + v \frac{\partial}{\partial x} \right)^2 w + D \frac{\partial^4 w}{\partial x^4} + Fw - N \frac{\partial^2 w}{\partial^2 x} = 0, \tag{3.1}$$

$$N = \frac{E}{2L} \int\limits_{-L/2}^{L/2} \left(\frac{\partial w}{\partial x} \right)^2 dx = \frac{6D}{L} \int\limits_{-L/2}^{L/2} \left(\frac{\partial w}{\partial x} \right)^2 dx,$$

where E is the Young's modulus of the pipe material. In many cases it is this nonlinear term (related to tension) that dominates during the growth of the perturbation amplitude and restricts this growth [14, 15]. The boundary and (zero) initial conditions are the same as in the linear case (see (2.2) and (2.3)).

3.2. Finite-difference scheme for the nonlinear problem. Let us rewrite equation (3.1) as follows:

$$D \frac{\partial^4 w}{\partial x^4} + (\rho_1 + \rho_2) \frac{\partial^2 w}{\partial t^2} + 2\rho_2 v \frac{\partial^2 w}{\partial x \partial t} + (\rho_2 v^2 - N) \frac{\partial^2 w}{\partial x^2} + Fw = f(x,t), \tag{3.2}$$

$$N = \frac{6D}{L}\int\limits_{-L/2}^{L/2}\left(\frac{\partial w}{\partial x}\right)^2 dx, \qquad F = (A + Bx^2)(\rho_1 + \rho_2).$$

All the derivatives appearing in equation (3.2) are approximated in the same way as in Subsection 2.3. To calculate the integral appearing in (3.2), we apply the following quadrature formula:

$$\int\limits_{-L/2}^{L/2} f(x)\,dx = f(x_0)\,h + \sum_{m=1}^{M-2}\frac{f(x_m) + f(x_{m+1})}{2}\,h + f(x_M)\,h, \qquad f(x_i) = \left(\frac{\partial w}{\partial x}(x_i)\right)^2.$$

Here

$$f(x_0) = \left(\frac{w_1 - w_0}{h}\right)^2 \qquad \text{and} \qquad f(x_M) = \left(\frac{w_M - w_{M-1}}{h}\right)^2$$

are the forward and backward differences, respectively, which approximate the integrand up to order $O(h)$, and

$$f(x_m) = \left(\frac{w_{m-1} - w_{m+1}}{2h}\right)^2, \qquad m = 1, \ldots, N-1,$$

is the central difference, which approximates the integrand up to $O(h^2)$. Then

$$N = \frac{6D}{L}\left[\frac{(w_1 - w_0)^2}{h} + \frac{1}{2}\sum_{m=1}^{N-2}\left(\frac{(w_{m-1} - w_{m+1})^2}{4h} + \frac{(w_m - w_{m+2})^2}{4h}\right) + \frac{(w_N - w_{N-1})^2}{h}\right]. \quad (3.3)$$

The value of N in the finite-difference equations was calculated in the intermediate, nth, time layer; therefore, the solution of the algebraic problem in the $(n+1)$th layer does not differ from that in the linear case.

The initial (2.6) and boundary (2.7) conditions, as well as the method of introducing the perturbation (2.8) for the nonlinear problem, are the same as in the linear case. Note that since we have $f(x_0) = f(x_m) = 0$ in view of the boundary conditions, the approximation of the integrand in N (3.3) is actually of order $O(h^2)$.

3.3. Results of calculations. At the first moments (while the amplitude remains small), the calculation of the nonlinear problem yields almost the same results as for the linear problem. For example, in Figs. 12 and 13 we plot the perturbations at the same time points as for the linear problem (Figs. 7 and 8). One can see that they are almost identical.

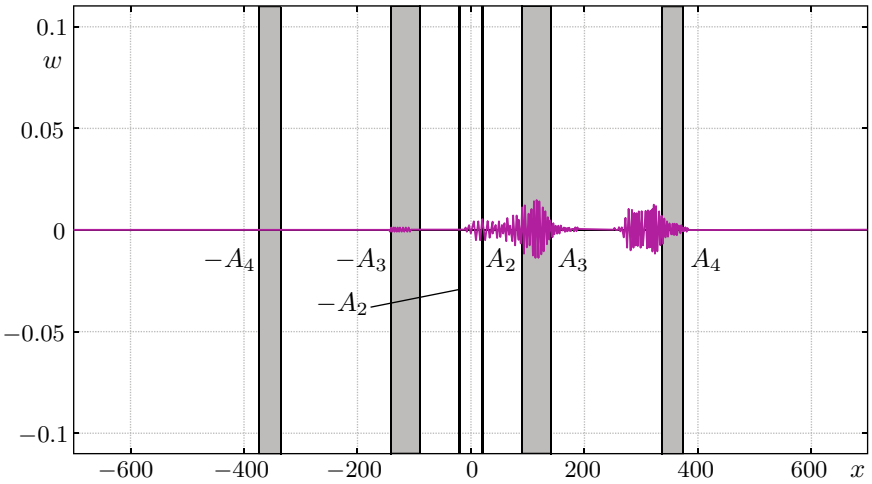

Fig. 12. Reflection from the points A_3 and A_4 in the nonlinear problem ($t = 59.5$).

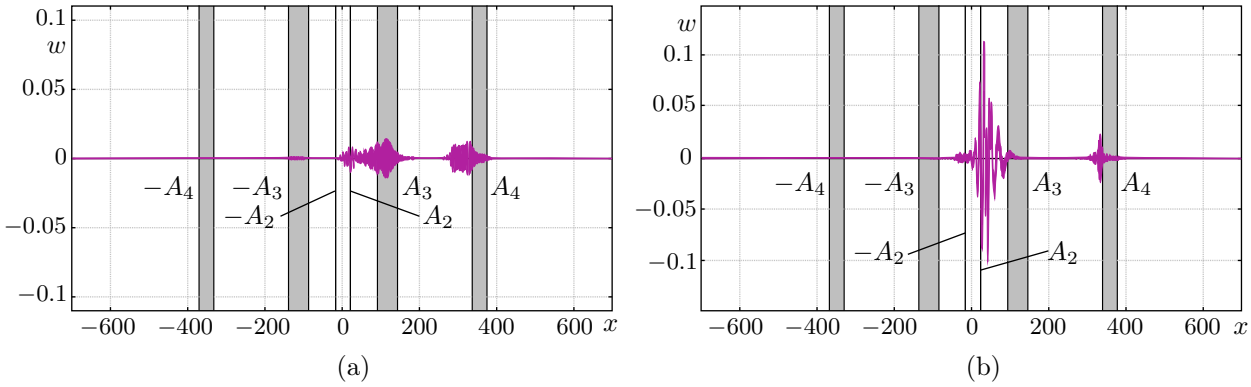

Fig. 13. (a) Beginning $t = 61$ and (b) end $t = 73.5$ of the growth of the perturbation in the nonlinear problem.

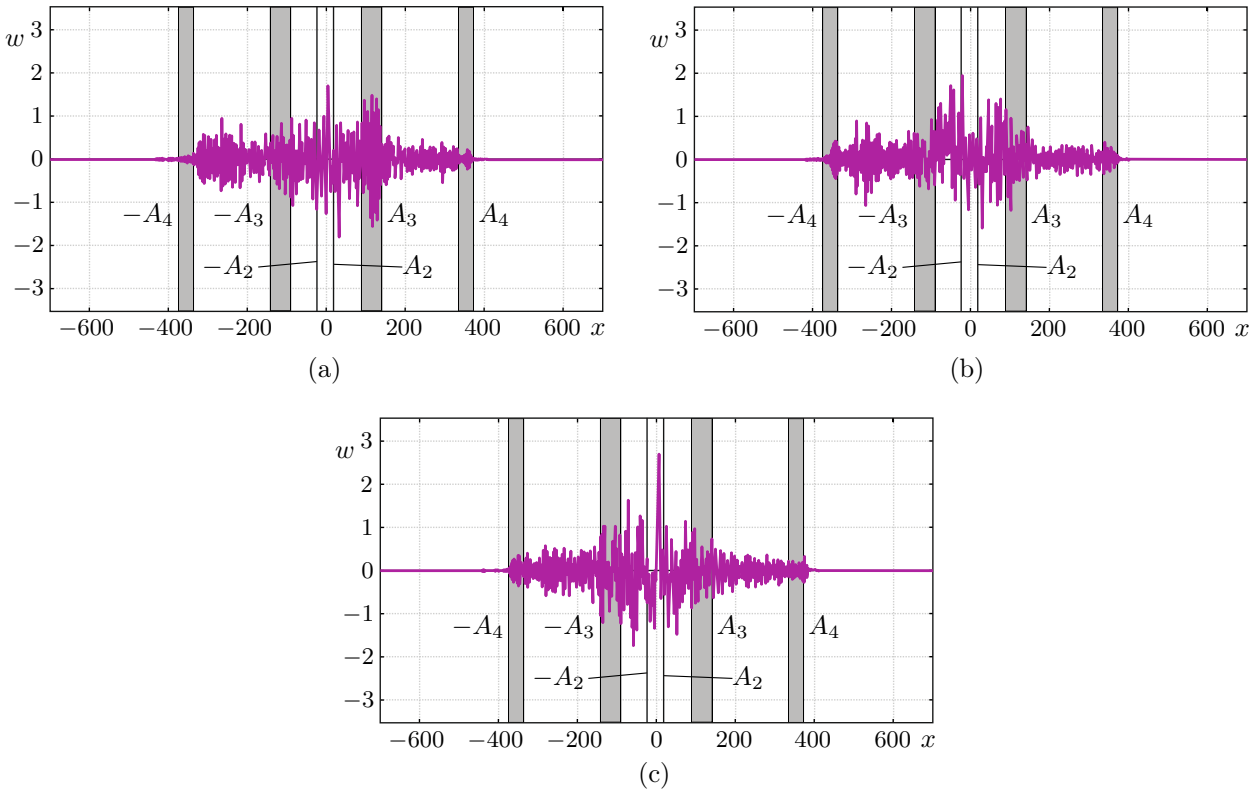

Fig. 14. Perturbation at the time points (a) $t = 2940$, (b) $t = 2970$, and (c) $t = 3000$.

Significant differences are observed after a long simulation time, $t > 126$, when the amplitude reaches a value of 1 or higher. From this time the perturbation amplitude in the nonlinear case is much lower than in the linear case, and its growth rate tends to zero with time. In the course of time the amplitude reaches a value on the order of 1 at all points of the interval $-A_4 < x < A_4$, which is drastically different from the situation in the linear problem (Fig. 11), where the amplitude reaches its maximum near the right boundary of the growth interval $(-A_2, A_2)$. It becomes difficult to visually identify the regular component of vibrations, and the motion becomes quasi-chaotic. The calculation of the nonlinear problem was carried out up to $t = 3000$, which is much longer than in the linear case ($t = 360$). The dynamics of the development of the perturbation at the final time points is shown in Fig. 14, where one can see that the bending of the pipe does not exceed 3 even after such a long time. It is worth noting that the perturbation does not leave the interval

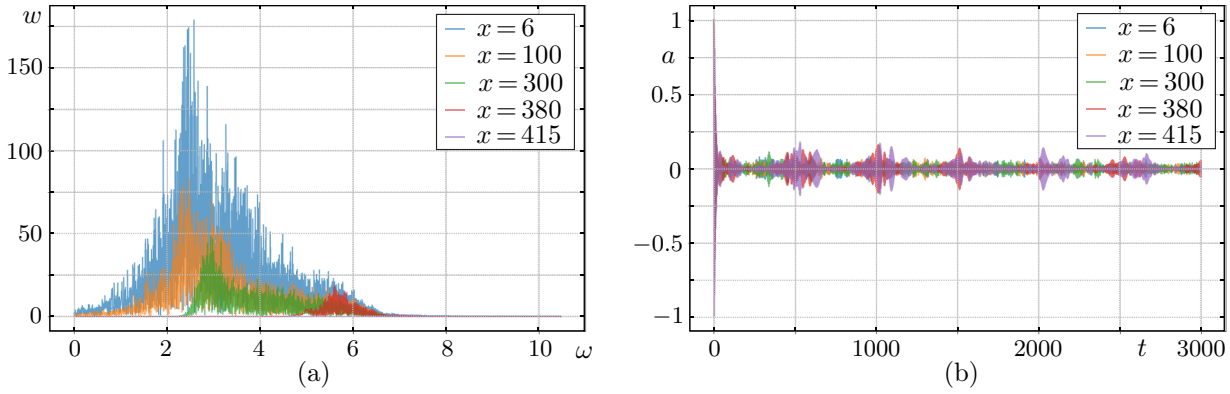

Fig. 15. Perturbation at different points: (a) spectrum and (b) autocorrelation function.

$-A_4 < x < A_4$ (where $A_4 = A_4(\omega)$) even in the nonlinear case; moreover, the amplitude in the interval $-A_3 < x < A_3$ is higher than that outside this interval; i.e., the internal reflection points retain their function even in the nonlinear case.

Figure 15 demonstrates the spectrum and the autocorrelation function of the perturbation for the nonlinear problem in the whole time range at the same points as in Subsection 2.4. One can see that the entire range of frequencies from 0 to 6.5 is present in the spectrum to a significant extent. At the center of the pipe the dominant frequency is lower than the initially introduced perturbation frequency, while away from the center the former is higher than the latter. The expansion of the range of frequencies involved in the perturbation (compared to the frequency range $\omega_0 < \omega < \omega_{\max}$ observed in the linear problem) and the redistribution of spectral amplitudes occur due to the nonlinear term in (3.1) and (3.2).

Figure 15b shows a slow decay of the autocorrelation function. Hence we can conclude that the regular component of the perturbation gradually disappears and the quasi-chaotic character of vibrations becomes more pronounced, which corresponds to the visually observed vibration process.

4. CONCLUSIONS

We have numerically simulated the propagation of a perturbation in a long pipe resting on a nonuniform elastic foundation and filled with a moving fluid. In this case the function describing the dependence of the wave number on the frequency has branch points, which determine the instability region and the internal reflection points in the pipe [6]. The development of the perturbation introduced into such a system was previously studied analytically in [6]. The results of our calculations of the linear problem correctly reproduce the analytical results of [6]. Namely, one can observe the main spatial regions that determine the structure of the growing eigenfunction: both the growth interval of the perturbation and the internal reflection points.

We have also numerically solved the nonlinear problem in which the dominant nonlinear tension of the pipe caused by its bending is taken into account. The results of calculations show that although the perturbation grows in the initial interval in the same way as in the linear problem, after reaching an amplitude on the order of 1 the growth of vibrations stops under the influence of nonlinear terms. The analysis of the character of vibrations, the spectrum, and the autocorrelation function reveals that the regular components of the perturbation decay with time and quasi-chaotic vibrations gradually start to dominate; moreover, the bending amplitudes of the pipe become of the same order of magnitude throughout the interval $-A_4 < x < A_4$. The nonlinearly developing perturbation in the interval $-A_3 < x < A_3$ has a higher amplitude than for $-A_4 < x < -A_3$ and $A_3 < x < A_4$, while outside the interval $-A_4 < x < A_4$ the perturbation exponentially decays away from this interval. Thus, the internal reflection points do not change their position and preserve

their function in the nonlinear case. In other words, although the perturbation in the nonlinear case develops in a significantly different way, its boundaries are determined by the linearized problem.

As pointed out in the Introduction, for linear systems of the second order in x (i.e., systems with two spatial waves) with variable coefficients, it was earlier proved that the presence of a region of local absolute instability is a necessary condition for the existence of a growing global linear eigenfunction [2, 8]. A similar result was obtained for a semi-infinite problem in the region $x > 0$ (see [4]). In this regard the results of [6], which have been confirmed numerically in the present study, show that this assertion is not generally true in the presence of more than two spatial waves. In fact the problem considered here is a counterexample: there exists a growing global eigenmode, but there is no local absolute instability at any point.

A different conclusion can be made in the case of nonlinear eigenmodes. Earlier the structures of nonlinear global eigenmodes for second-order systems were studied based on the Ginzburg–Landau model equation. There were distinguished "soft" modes [11], in which the amplitude varies slowly as a function of the coordinate, and "steep" modes [13], in which a rapid growth of the amplitude occurs at one of the edges defined by the boundary of the linear absolute/convective instability region. The soft nonlinear modes result from the development of growing global linear eigenmodes, while the steep modes may arise even in the absence of global linear instability [12]. A global eigenmode of similar structure was constructed in the case of the semi-infinite region $x > 0$ (see [4]) on the basis of the same model equation.

An important feature of the nonlinearity considered in the cited papers is its local character, which has allowed the authors to obtain a nonlinear local dispersion equation and to construct asymptotic structures of global nonlinear eigenmodes using a generalization of the WKB method. In all cases it turned out that the boundary of the region occupied by the eigenmode is determined by purely linear properties of the problem. In other words, nonlinear phenomena manifest themselves in a developing perturbation up to its saturation (cessation of growth) but do not affect its boundaries. In the present study, we have obtained exactly the same result: a developed nonlinear perturbation does not leave the region $-A_4 < x < A_4$ defined by the linear problem even after passing to the quasi-chaotic regime, and in the region $-A_3 < x < A_3$ (whose boundaries reflect part of the waves in the linear case) this perturbation has a higher amplitude. Moreover, the nonlinearity considered in the present study is essentially nonlocal (it integrally depends on the deformation of the pipe throughout its length); therefore, analytical constructions similar to those in [4, 11–13] are impossible in principle in this case. We can conjecture that the edges of the developed nonlinear perturbation will only be governed by the linear problem in a much more general situation than that considered in [4, 11–13].

ACKNOWLEDGMENTS

We are grateful to A. G. Kulikovskii for his interest in the study and useful discussions.

FUNDING

The work of the second author (Sections 1, 2, and 4) was supported by the Russian Science Foundation under grant no. 19-71-30012, https://rscf.ru/project/19-71-30012/, and performed at the Steklov Mathematical Institute of Russian Academy of Sciences.

REFERENCES

1. N. S. Bakhvalov, A. A. Kornev, and E. V. Chizhonkov, *Numerical Methods: Problem Solutions and Exercises* (Drofa, Moscow, 2009) [in Russian].
2. J.-M. Chomaz, P. Huerre, and L. G. Redekopp, "A frequency selection criterion in spatially developing flows," Stud. Appl. Math. **84** (2), 119–144 (1991).

3. W. Coenen, L. Lesshafft, X. Garnaud, and A. Sevilla, "Global instability of low-density jets," J. Fluid Mech. **820**, 187–207 (2017).
4. A. Couairon and J.-M. Chomaz, "Fully nonlinear global modes in slowly varying flows," Phys. Fluids **11** (12), 3688–3703 (1999).
5. V. I. Feodos'ev, "On the vibrations and stability of a pipe with liquid flowing through it," Inzh. Sb. **10**, 169–170 (1951).
6. A. G. Kulikovskii, "On the stability loss of weakly non-uniform flows in extended regions. The formation of transverse oscillations of a tube conveying a fluid," J. Appl. Math. Mech. **57** (5), 851–856 (1993) [transl. from Prikl. Mat. Mekh. **57** (5), 93–99 (1993)].
7. A. G. Kulikovskii and I. S. Shikina, "On bending vibrations of a long pipe filled with a moving fluid," Izv. Akad. Nauk ArmSSR, Mekh. **41** (1), 31–39 (1988).
8. S. Le Dizès, P. Huerre, J. M. Chomaz, and P. A. Monkewitz, "Linear global modes in spatially developing media," Philos. Trans. R. Soc. London A **354** (1705), 169–212 (1996).
9. P. A. Monkewitz, "The absolute and convective nature of instability in two-dimensional wakes at low Reynolds numbers," Phys. Fluids **31** (5), 999–1006 (1988).
10. B. Pier, "On the frequency selection of finite-amplitude vortex shedding in the cylinder wake," J. Fluid Mech. **458**, 407–417 (2002).
11. B. Pier and P. Huerre, "Fully nonlinear global modes in spatially developing media," Physica D **97** (1–3), 206–222 (1996).
12. B. Pier, P. Huerre, and J.-M. Chomaz, "Bifurcation to fully nonlinear synchronized structures in slowly varying media," Physica D **148** (1–2), 49–96 (2001).
13. B. Pier, P. Huerre, J.-M. Chomaz, and A. Couairon, "Steep nonlinear global modes in spatially developing media," Phys. Fluids **10** (10), 2433–2435 (1998).
14. A. Shishaeva, A. Aksenov, and V. Vedeneev, "The effect of external perturbations on nonlinear panel flutter at low supersonic speed," J. Fluids Struct. **111**, 103570 (2022).
15. V. V. Vedeneev, "Limit oscillatory cycles in the single mode flutter of a plate," J. Appl. Math. Mech. **77** (3), 257–267 (2013) [transl. from Prikl. Mat. Mekh. **77** (3), 355–370 (2013)].
16. V. V. Vedeneev and A. B. Poroshina, "Stability of an elastic tube conveying a Non-Newtonian fluid and having a locally weakened section," Proc. Steklov Inst. Math. **300**, 34–55 (2018) [transl. from Tr. Mat. Inst. Steklova **300**, 42–64 (2018)].
17. A. S. Vol'mir, *Nonlinear Dynamics of Plates and Shells* (Nauka, Moscow, 1972) [in Russian].

Translated by I. Nikitin